Determination of Stresses Around Beads in Stressed Epoxy Resin by Photoelasticity

Andrzej Pawlak, Andrzej Galeski

Centre of Molecular and Macromolecular Studies, Polish Academy of Sciences, Sienkiewicza 112, Lodz, Poland

Received 25 April 2001; accepted 2 April 2002

ABSTRACT: Microphotoelasticity gives the possibility of determining stresses in systems with small inclusions. We studied four systems with the same matrix (epoxy resin) and different inclusions of spherical shapes. The distributions of stresses and pressure, after the application of external tensile forces, were determined. In a matrix with a hard inclusion, tensile stresses concentrated at the pole. For a soft inclusion, that is, a poly(vinyl acetate) bead or an air bubble, the tensile stresses concentrated at the equator with some compression at the pole. The soft inclusion promoted the stress relaxation by the change in its shape. In the matrix with a stiff inclusion, such as a steel or glass bead, debonding was observed at the interface near the pole area. In such a case, the stress concentration region moved toward the tip of the debonding. For a hard inclusion, the pressure at all points of the interface was negative, and the maximum was found at the pole near the inclusion surface from −6 to −10 MPa. This region was sensitive to the initiation of destruction processes such as cavitation and debonding. For a soft inclusion, the pressures at the pole and equator were comparable, but the signs were opposite, being positive at the pole (compression) and negative at the equator (expansion). © 2002 Wiley Periodicals, Inc. J Appl Polym Sci 86: 1436–1444, 2002

Key words: stress; resins; mechanical properties; fillers; heterogenous polymers

INTRODUCTION

The mechanical properties of composite materials and blends strongly depend on the dispersion and shape of a minor phase. It is known that during the deformation of nonhomogeneous materials, stresses concentrate at certain locations in the matrix, usually near the interphase boundary and at edges. The failure processes are normally initiated in the stressed area, so a knowledge of stress distributions seems to be of great importance.

Theoretical calculations of stresses in a matrix with a single spherical inclusion subjected to uniaxial tension were conducted by Goodier[1] in the 1930s. An assumption of perfect adhesion was used in this approach. Edwards[2] extended the calculations to cases of hydrostatic stress and plane shear. Much later, Hashin[3] presented a more general description, including the influence of the inclusion being coated with a thin layer of a third component. His theoretical considerations were verified by computer simulations. Guild and Young[4,5] used finite elements to determine stress concentrations in epoxy composites with different amounts of glass beads.

The mechanical properties of polymers filled with spherical inclusions are described and discussed in many research articles.[6–11] Abate and Heikens[11] analyzed the formation of cracks in polystyrene with glass beads under axial tension. They observed a strong dependence of the cracking position near the interface on adhesion.

The main conclusion of those experimental studies is that the mechanical properties are strongly influenced by the character of the interaction between the inclusions and the matrix and, therefore, are similar in systems with similar types of interactions. The interaction depends on the adhesion between components, the ratio of Young's moduli for the matrix and inclusion, and the ratio of Poisson coefficients.

The sensing of stresses in a material by photoelasticity is quite versatile and is widely used among experimental methods.[12] A popular frozen-stress version requires the preparation of three models that are cut into thin slices and then carefully analyzed by two-dimensional photoelasticity, one after another. Some years ago, we developed a photoelastic method that could be used for the determination of the stress distribution without destruction of the analyzed sample.[13] The method is based on the deconvolution of the information on the changes in the phase and polarization of light passing through the sample. The sample is virtually divided into thin slices (optical elements), each described by a matrix with characteristic retardation and characteristic angles. We also applied Aben's concept of equivalence theorem.[14,15] The de-

Correspondence to: A. Galeski (andgal@bilbo.cbmm.lodz.pl).
Contract grant sponsor: Polish State Committee for Scientific Research; contract grant number: 7 T08E 03914.

veloped method is limited to axially symmetrical systems. An example of stress determination in an epoxy matrix including a spherical inclusion was shown, and the applicability of the method was verified by a comparison with Goodier's prediction of the stress distribution around a sphere embedded in a matrix.[13] We applied our photoelastic method to the analysis of residual stresses around microspherical inclusions in an epoxy matrix. The observed differences between the theory and experiments were results of interface influence, which is not considered in the theory.[16]

In this article, we discuss how the stress state depends on the type of inclusion present in the matrix and how the stress distribution changes after debonding.

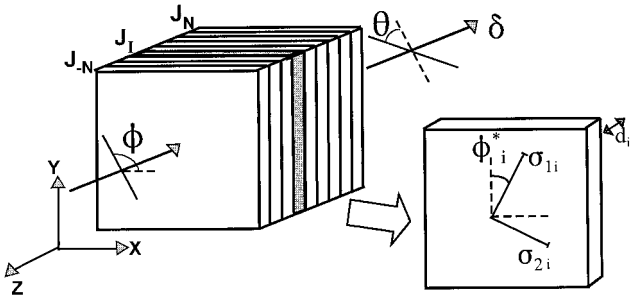

Figure 1 Scheme of the passage of light through a photoelastic model characterized by two characteristic directions, ϕ and θ, and a characteristic retardation, δ. The model is divided into $2N + 1$ birefringent plates with secondary principal stresses σ_{1i} and σ_{2i} in the ith plate.

EXPERIMENTAL

Short description of the method

The method was described previously,[13] but a short summary seems to be necessary for a better understanding of the experiments.

The alteration of the phase and polarization of light transmitted through a three-dimensional photoelastic sample is described by three measurable parameters: the primary and secondary characteristic directions (ϕ and θ) and the characteristic retardation ($\delta = 2\delta'$). They are incorporated into the elements of a Jones matrix defined for the whole sample:

$$\boldsymbol{C} = \begin{bmatrix} \cos\delta'\cos\theta + i\sin\delta'\cos(2\varphi+\theta) & -\cos\delta'\sin\theta + i\sin\delta'\sin(2\varphi+\theta) \\ \cos\delta'\sin\theta + i\sin\delta'\sin(2\varphi+\theta) & \cos\delta'\cos\theta - i\sin\delta'\cos(2\varphi+\theta) \end{bmatrix} \quad (1)$$

According to the equivalence theorem, the complicated optical object **C** can be represented by an assembly of $2N + 1$ birefringent plates. Each of these plates represents local optical properties $\mathbf{J}_i$, which depend on the stress components in a plane perpendicular to the light propagation (σ_{1i} and σ_{2i}; see Fig. 1). The matrix **C** is then the multiplication of matrices, each related to a particular birefringent plate (retarder):

$$C = J_N J_{N-1} \ldots J_i \ldots J_1 J_0 J_{-1} J_{-2} \ldots J_{-N} \quad (2)$$

The matrix $\mathbf{J}_i$ has the following form:

$$\boldsymbol{J}_i = \begin{bmatrix} \cos\delta_i - i\sin\delta_i\cos 2\varphi_i^* & i\sin\delta_i\sin 2\varphi_i^* \\ i\sin\delta_i\sin 2\varphi_i^* & \cos\delta_i + i\sin\delta_i\cos 2\varphi_i^* \end{bmatrix} \quad (3)$$

where the secondary principal stress direction ϕ_i^* is measured from the y axis. The secondary retardation in the i plate, $2\delta_i$, is equal to

$$\delta_i = \pi * \Delta\sigma_i * d_i / K \quad (4)$$

where $\Delta\sigma_i = \sigma_{1i} - \sigma_{2i}$ is the difference of secondary principal stresses, d_i is the thickness of the plate, and K is the photoelastic constant.

The purpose of the experiment is the determination of the distribution of directions and the values of primary principal stresses from the changes in the polarization of transmitted light, such as the determination of the stress tensor at each point of the studied sample. The problem concerns the $(2N + 1) \times 3$ unknown components of the stress tensor in its diagonal form and the $(2N + 1) \times 2$ unknown directions of principal stresses. Because in a single measurement only three values (ϕ, θ, and δ) are determined, it is necessary to reduce the number of independent variables. The following restrictions should sufficiently limit the number of unknown parameters to be determined:

- There is only one isolated inclusion in the matrix, and the others are far from the considered inclusion.
- The load applied to the sample preserves the axial symmetry of the system.
- The stress far from the inclusion is homogeneous.
- The region of the sample around the inclusion is divided into two zones, one near the inclusion, where significant stress concentration is expected, and the other far from the inclusion, where stresses are uniform and related to the externally applied force.
- The stress in the uniformly stressed zone is easy to determine from eq. (4) because the material on a light path is represented by a single birefringent plate:

$$\sigma_j = \frac{K * \delta}{2\pi * D} \quad (5)$$

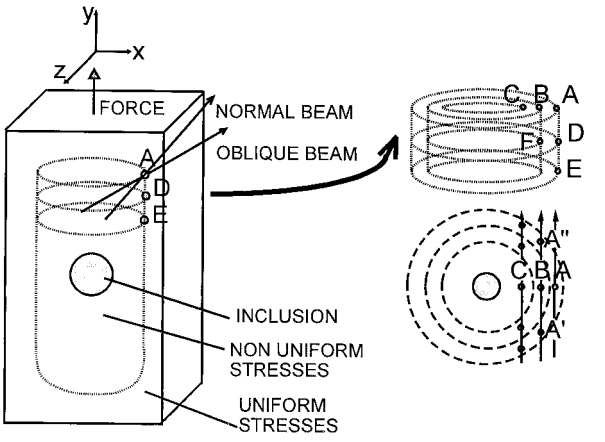

Figure 2 Photoelastic model and its partitions into shells.

where D is the thickness of the sample. The characteristic retardation can be easily measured.

Near the inclusion, the uniformity of stress is disturbed. It follows from the axial symmetry of the system that the stresses can be determined only at points in the main plane, such as the plane that includes the symmetry axis. Stresses in other points of the nonuniform area are identical to stresses at points of the main plane. The region with disturbed stresses may be divided into thin concentric shells. The light path through the sample consists of sectors in uniform part and sectors assigned to elements of shells. Each sector may be treated as a birefringent plate [eq. (3)].

The analysis begins from the light beam that passes through uniform areas and a single element A from the outer shell of stressed areas (Fig. 2). In Jones's calculus, it is equivalent to the passage of light through three retarders. Two of them, representing uniform areas, are known. If the characteristic parameters for the system of three retarders are measured, it is possible to determine from eq. (2) the characteristic parameters, ϕ_i^*, and δ_i, for element A. It is then possible to calculate the difference in the secondary principal stresses ($\Delta\sigma_A$) and their direction in the plane perpendicular to the light-beam direction. Because A is the element on the plane including the symmetry axis, one of the principal stresses is perpendicular to this plane, and two others are equivalent to secondary stresses.

The polarization of light is not sensitive to the stress component parallel to the propagation direction; however, the third principal stress can be determined by the illumination of the sample at some acute angle Ω. With a procedure similar to that for normal illumination, it is possible to determine $\Delta\sigma'_A$ for the oblique direction.

If those steps are followed for other points (D and E in Fig. 2), the stress difference $\Delta\sigma$ for all elements of the cylindrical shell can be determined. The individual stress components are separated at the end of the calculation procedure from their differences on the basis of an equilibrium equation for the system.

The next step in the analysis is the determination of the polarization of a beam passing through element B in a more inner shell. The beam passes through the uniformly stressed region, elements A′, B, and A″, and finally through the second uniformly stressed region. The stresses in elements A′ and A″ are the same as those in A, but a different orientation with respect to the coordination axis must be taken into account. Only the stresses in the B element are unknown. We can determine them in a fashion similar to that used for element A on the basis of eq. (2) and with knowledge of the stresses in other elements.

In the same way, the stresses at other points of the shell (e.g., F and G) may be determined. Continuing this procedure, we finally can calculate the stresses at all points of the main plane; this is equivalent to the knowledge of the stress distributions in the whole sample. The individual stress components are separated from their differences on the basis of an equilibrium equation for the system.

Micropolariscope and materials

For stress determination with our method, it is necessary first to measure the characteristic parameters that can be accomplished simultaneously for many light beams with the micropolariscope presented in Figure 3. The micropolariscope, built on the basis of a polarizing microscope, was connected to a CCD TV (Panasonic BL 202) camera installed in the place of an eyepiece.[13,16] The illuminating light was filtered with a monochromatic filter (λ = 546 nm). The initial light polarization was modified by stresses inside the sample and then by a quarter-wave plate and an analyzer, both having a known orientation. A photoelastic image was registered and transmitted to a computer. The camera image had a 577 × 581 pixel resolution and 256 gray levels. The sample was placed in a small tensile machine mounted on the microscope stage. After the application of a load, the sample elongation was measured, and the uniform stress within the sample was

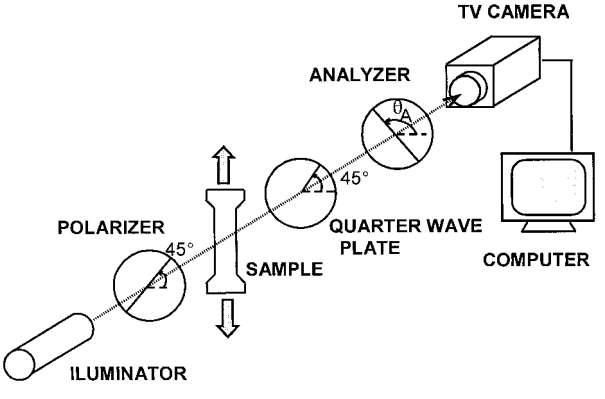

Figure 3 Scheme of the micropolariscope.

determined. The tensile device had the ability to tilt to change the orientation of the stressed sample with respect to the light-beam direction, that is, to have oblique illumination.

The measurement of the characteristic directions was based on Aben's definition.[15] In this case, the quarter-wave plate was removed from the experimental setup. The intensity of transmitted light became minimal when the polarizer was parallel to the primary principal direction (ϕ) and the analyzer was perpendicular to the secondary principal direction ($\phi + \theta$). By rotating both these optical elements and recording the intensities for all points of the image, we could measure the characteristic directions for all necessary light rays at the same time.

The characteristic retardation was determined with a modified Senarmont method.[17] In this method, the polarizer and the quarter-wave plate were oriented at an angle of 45° with respect to the x axis, and the analyzer was rotated by the θ_A angle. The intensity of light for each analyzer position was measured. The orientation θ_{AM}, corresponding to the minimum, was used for the determination of the characteristic retardation δ according to the following equation:

$$\tan 2\theta_{AM} = \frac{\cos^2\delta(\cos^2\theta - \sin^2\theta) - \sin^2\delta(\cos^2\beta - \sin^2\beta)}{2 \sin \delta \cos \delta \cos 2\varphi} \quad (6)$$

where β is $2\phi + \theta$.

The micropolariscope was employed for the determination of characteristic parameters around isolated spherical inclusions embedded in an epoxy resin matrix. Several types of microspheres were used: glass, steel, and poly(vinyl acetate) (PVA) beads. The diameter of the glass and steel beads was 250 μm, whereas the diameter of PVA inclusions approached 400 μm. The epoxy matrix was formed by the curing of Araldite 502 (Polysciences) resin with a dodecenyl succinic anhydride hardener in the presence of a 2,4,6-tri(dimethylamino ethyl) accelerator. The curing procedure consisted of a few steps necessary for the preparation of a sample without noticeable residual stresses. First, a mold in the shape of a dog bone was half-filled with a thin layer of epoxy (200–300 μm) that was precured for 2 h at 75°C under pressure reduced by 0.06 MPa. The viscosity of a resin increases during curing, so it was possible to place the inclusion on the top of this layer and then to fill up the mold with the rest of resin, which was also previously heated for 2 h at 75°C. Final curing was performed in three steps: 1 h at 75°C, 16 h at 40°C, and 72 h at 30°C. The steps for the curing temperature minimized the residual stresses. The material properties of the cured resin and inclusions are summarized in Table I.

Dog-bone-shaped samples with a gauge length of 30 mm and a cross section of 7 mm × 1 mm were deformed in tension to a 1.5–3% strain, that is, in the range of the linear response of an epoxy matrix (up to 3%). The deformed sample was illuminated in two directions of light: perpendicular to the sample surface and oblique (15–20°) from the normal to the surface. Characteristic parameters were determined from the images recorded for different orientations of the micropolariscope elements. These parameters were used for computer calculations of stresses around inclusions.

TABLE I
Characteristics of Materials

Component	Inclusion size (μm)	Elastic modulus (GPa)	Poisson ratio
Cured epoxy resin	—	1.4	0.36
Glass beads	250	70.0	0.22
Steel beads	250	200.0	0.28
PVA beads	400	1.0	0.40

RESULTS AND DISCUSSION

Hard inclusions: steel and glass

A steel bead is an example of a hard inclusion with good adhesion to an epoxy matrix. The load applied to the sample in the vertical (y) direction produced a uniform tensile stress of 11.2 MPa.

The stresses around inclusions were determined from the characteristic parameters for normal and oblique illumination, which are presented in Figure 4. The disturbance of the primary direction is not greater than 4° from the tensile deformation direction. The secondary direction angle is between −1 and +2°. Very different from uniformity are the maps of the characteristic retardation. The values in the matrix near the pole (on top of the inclusion and on the symmetry axis) and near the equator are significantly larger than in the uniform stressed area (far from the inclusion). The measured retardation has a minimum absolute value in the zone located 45° from the tensile deformation direction.

Three main components of the stress tensor and the orientation of σ_1 in relation to the x axis (horizontal), calculated from characteristic parameters, are presented in Figure 5. Because of the symmetry of the system, only quarters of the main plane are shown. Two principal stresses, σ_1 and σ_2, are in the plane of drawing; the third, σ_3, is perpendicular to the page. Typically, the σ_2 direction is not far from the applied force direction (y). σ_1, by definition, is perpendicular to σ_2. The deviation of σ_1 from the horizontal direction does not exceed 9° from the inclusion and is larger only very close to the interface. Stresses concentrate near the pole of inclusion, and they are tensile. The σ_2

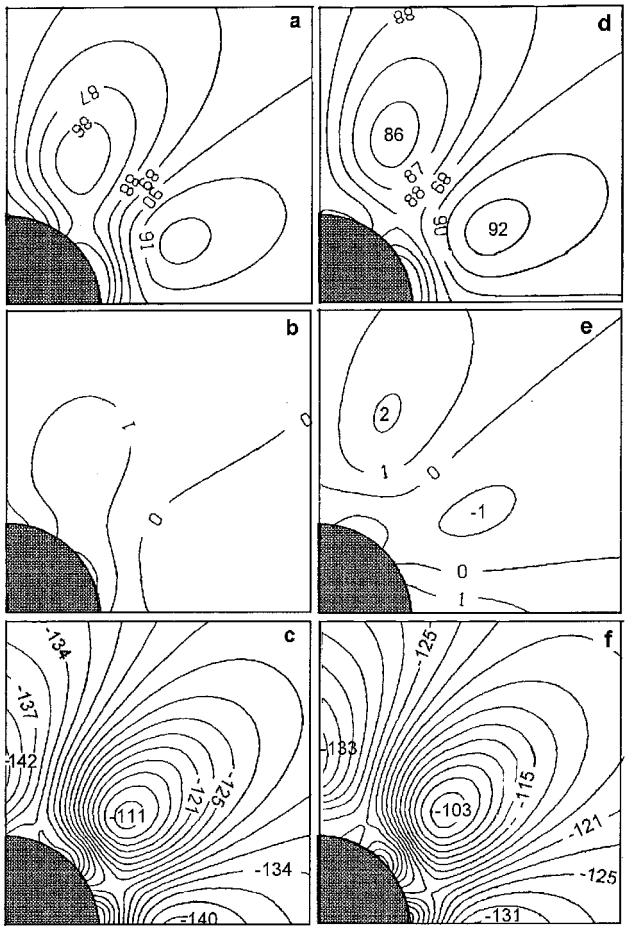

Figure 4 Characteristic parameters around a steel bead embedded in an epoxy matrix stretched with 11.2 MPa: (a) the primary characteristic angle, (b) secondary characteristic angle, and (c) characteristic retardation for the perpendicular illumination of the sample surface and (d) the primary characteristic angle, (e) secondary characteristic angle, and (f) characteristic retardation for the oblique illumination. All values are in degrees. Only quarter parts of full images are presented, with part of the inclusion in the lower left corner. Other parts are symmetric in relation to the horizontal and vertical axes. The direction of deformation is vertical.

component near the inclusion is nearly twice as large as the externally applied stress (20.8 MPa). It is interesting to note the negative values of σ_1 and σ_3 near the equator of the inclusion. Negative values represent compression. This means that there is a tendency from the matrix to stretch the steel inclusion at the pole and compress it at the equator. The stress-concentrated zone extends in the matrix for a distance larger than two radii of inclusion. The tendency of stretching the matrix at the pole is confirmed by the observation of the pressure distribution [Fig. 5(e)]. The values of pressure were determined with the following equation:

$$p = -\frac{\nu}{\nu + 1}(\sigma_1 + \sigma_2 + \sigma_3) \qquad (7)$$

where ν is the Poisson coefficient.

Maximum negative pressure is found at the pole near the inclusion surface at the level of -10 MPa. Therefore, this region is sensitive to the initiation of destruction processes such as cavitation and debonding.

We compared the determined values of stresses with those predicted by Goodier's theory,[1] using for the theoretical calculations the parameters from our experiment, which are listed in Table I. The stress maps are very similar (they are not shown here), and there is a fair agreement of our numerical data with the Goodier theory; however, the measured values are slightly lower at the pole and slightly higher at the equator (see Table II). These differences are probably the results of nonperfect adhesion, which makes possible some mechanical relaxation at the pole.

The second example of a hard inclusion in a softer matrix is a glass bead embedded in an epoxy. In this case, the state of stress under applied tension is similar to that for a steel inclusion. The stress distributions in

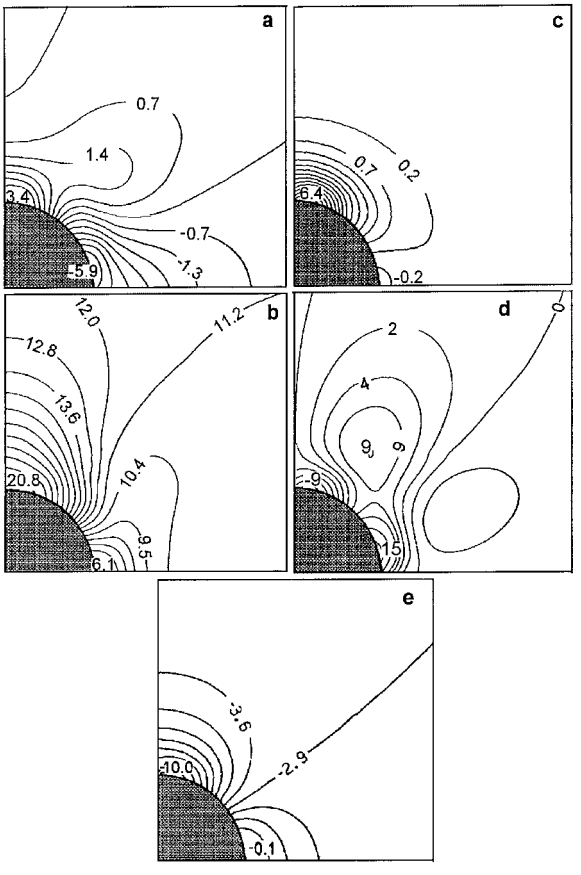

Figure 5 Principal stresses and their direction in an epoxy matrix around a steel bead (the sample was stretched with 11.2 MPa): (a) σ_1, (b) σ_2, (c) σ_3, (d) the angle between the horizontal axis and σ_1 direction, and (e) the pressure. Stresses and pressures are given in megapascals, and angles are given in degrees. Only quarter parts of full images are presented, as in Figure 4.

TABLE II
Comparison of the Maximum Values of Principal Stresses Determined for the Steel Inclusion from the Experiment and with Goodier's Theory

Position	σ_1 (MPa)	σ_2 (MPa)	σ_3 (MPa)
Pole (experiment)	3.4	20.8	6.4
Pole (Goodier)	4.1	22.2	4.1
Equator (experiment)	−5.9	6.1	−0.2
Equator (Goodier)	−4.2	5.9	−0.2

TABLE III
Comparison of the Maximum Values of Principal Stresses Determined for the Glass Inclusion from the Experiment and with Goodier's Theory

Position	σ_1 (MPa)	σ_2 (MPa)	σ_3 (MPa)
Pole (experiment)	1.5	18.0	7.0
Pole (Goodier)	4.0	22.5	4.0
Equator (experiment)	−2.9	8.8	−0.9
Equator (Goodier)	−4.0	6.5	−0.2

the matrix are presented in Figure 6. The applied uniform stress was 11.5 MPa. The stress concentration near the pole is slightly lower than in the previous case: the maximum value of principal stress σ_2 is 18.0 MPa, and the maximum negative pressure is −6.6 MPa. All stress components near the pole have positive values. On the equatorial part of the matrix, some compression is observed, but it is weaker than that for the steel bead. Just as for the steel bead, the recorded pressures at all points are negative, but the distribution is more uniform than for the steel inclusion. These changes in the stresses and pressure are probably the results of material properties, such as a lower Young's modulus of inclusion and different adhesion. A comparison of the measured values of stresses with those calculated according to the Goodier theory is presented in Table III. Observed differences are probably the results of some relaxation at the pole due to limited adhesion between the glass bead and the polymer matrix.

During tensile deformation of an epoxy matrix with glass inclusions, the debonding around one of the poles of inclusion is usually observed above 1–2% deformation, whereas the debonding between steel and epoxy is usually observed at a strain larger than 2%. The debonding process is fast and easily recognizable from the changes in the photoelastic image. Exemplary photoelastic images, observed when the stretched sample was placed between crossed polarizers, are shown in Figure 7.

The stress distributions in the matrix after debonding near one pole, determined from the characteristic retardation and primary and secondary angles, are presented in Figure 8. In this sample, the loss of contact at one pole was observed when the applied stress reached 15 MPa. Microscopic observations showed that the stresses on the opposite pole are usually only little affected by the debonding. The stresses in the epoxy matrix, close to the sector in which the contact was lost, were relaxed, and the matrix here is even less deformed than in the region far from the inclusion

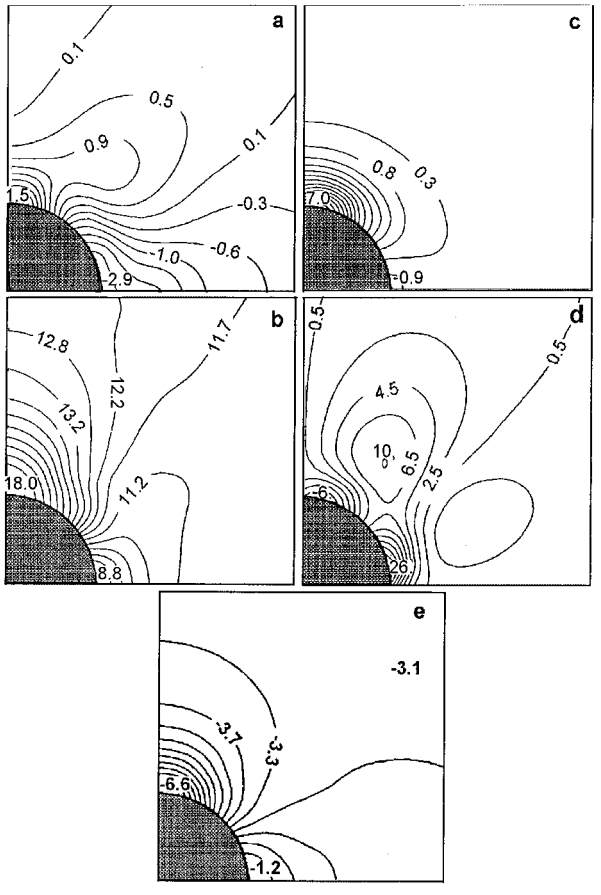

Figure 6 Principal stresses and their direction in an epoxy matrix around a glass bead (the sample was stretched with 11.5 MPa): (a) σ_1, (b) σ_2, (c) σ_3, (d) the angle between the horizontal axis and σ_1 direction, and (e) the pressure.

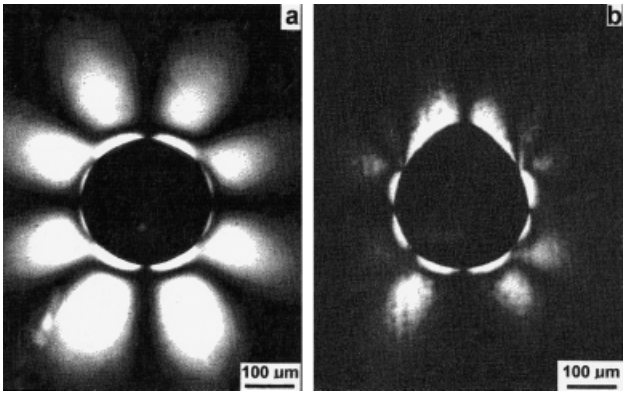

Figure 7 Photoelastic images of a glass bead inside an epoxy matrix (a) before and (b) after debonding at the upper pole. The direction of deformation is vertical. The elongations of the sample were 1 and 3%, respectively.

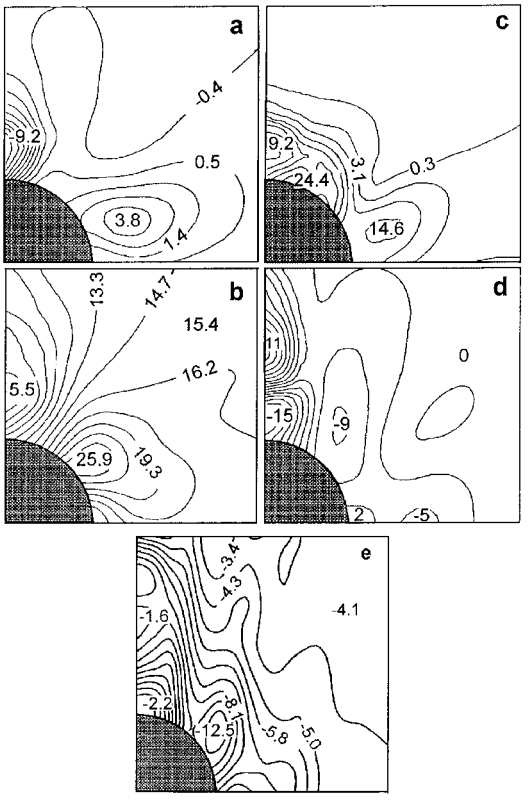

Figure 8 Stress distributions near a glass bead after debonding: (a) σ_1, (b) σ_2, (c) σ_3, (d) the angle between the horizontal axis and σ_1 direction, and (e) the pressure.

compressed here. The position of the most stressed zone shifted to 40° away from the y axis, near the debonding tip. In this place, both components σ_2 and σ_3 have high values of 24–26 MPa, that is, 70% more than the stress applied to the sample. The maps of stress components, presented in Figure 8, in their equatorial zones resemble the maps for a hard inclusion (cf. Fig. 6), whereas in pole regions the maps are characteristic for a soft inclusion (see the next section). The maximum of the negative pressure is present at a position around 45–50° from the vertical axis and is at a quite high level of −12.5 MPa.

If the deformation of the sample is continued, the crack tip propagates slowly along the interface, and the stress concentration area shifts toward the 45° position. When the total deformation reaches 2–3%, debonding near the second pole is observed.

Soft inclusions: PVA beads and air bubbles

The PVA bead is an example of an inclusion softer than the harder epoxy matrix (see Table I); however, the difference in the elastic moduli is not very large. The sample was stretched with 5.6 MPa. Observations of characteristic parameters show a trend opposite to that for the hard inclusion (see Fig. 9). The values of the primary characteristic angle are between 89 and 92°. The deviations of the secondary characteristic parameters from the neutral value 0 were larger than those observed for samples with steel and glass beads. The measured characteristic retardations show that PVA and hard inclusions have opposite tendencies. The retardation near the pole and the equator is lower than in the uniformly deformed part of the matrix. Near the inclusion, at the 45° position, the retardation is approximately 10% larger.

The measured retardation values have a range similar to that for hard inclusions, and this is due to the larger size of the PVA bead; the region of concentrated stresses is also more extended, despite the lower applied stress.

The results of the stress component calculations are presented in Figure 10. A positive pressure in the matrix near the pole is visible at the level of 1 MPa [Fig. 10(e)], which is accompanied by the tensile stress near the equator [Fig. 10(b)]. The maximum value of

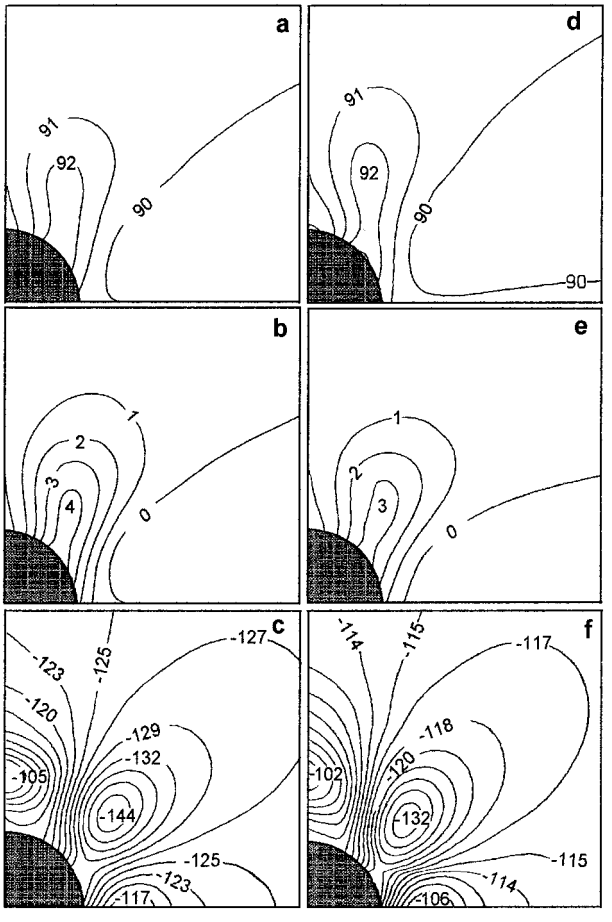

Figure 9 Characteristic parameters around a PVA bead embedded in an epoxy matrix stretched with 5.6 MPa: (a) the primary characteristic angle, (b) secondary characteristic angle, and (c) characteristic retardation for the perpendicular illumination of the sample surface and (d) the primary characteristic angle, (e) secondary characteristic angle, and (f) characteristic retardation for oblique illumination. All values are in degrees.

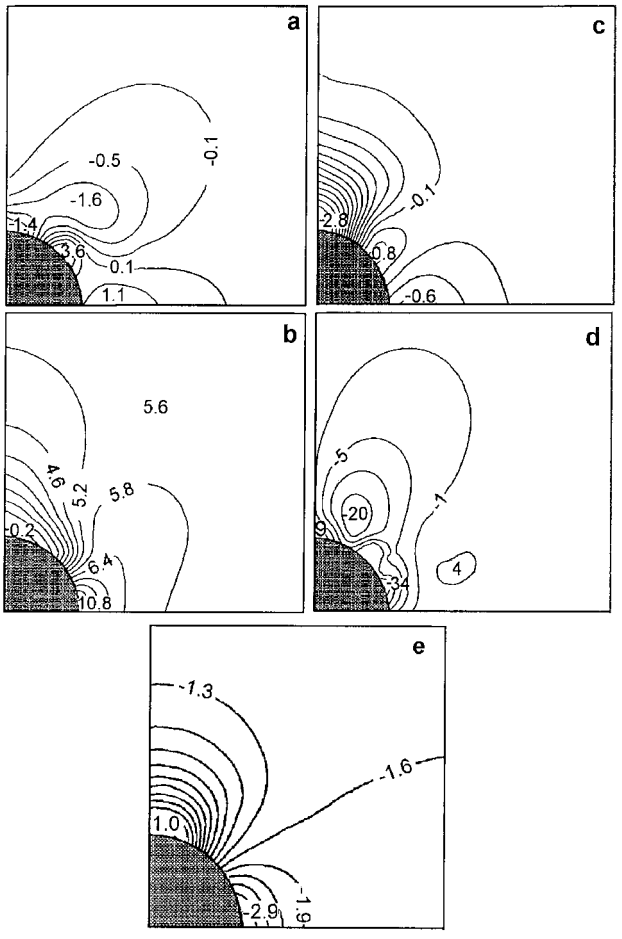

Figure 10 Principal stresses and the direction in an epoxy matrix around a PVA inclusion (the sample was stretched with 5.6 MPa): (a) σ_1, (b) σ_2, (c) σ_3, (d) the angle between the horizontal axis and σ_1 direction, and (e) the pressure.

the tensile stress component reaches the level of 10.8 MPa. At the equator, the two stress components in the matrix are tensile, whereas the third is slightly compressive. A large change in stress directions should be noted [Fig. 10(d)]. The significant nonuniformities of stresses are visible not farther than two radii from the inclusion surface. The character of the stresses suggests that the partial relaxation at the pole is due to the significant mechanical compliance of the inclusion; the total elongation of the sample was less than 1%, so it was difficult during microscopic observation to notice small changes in the inclusion shape.

We compared the measured values of the stresses with those predicted by Goodier's model (see Table IV). There is a general agreement, but we observe higher compression at the pole and stronger tensile deformation at the equator. These differences may be explained by small changes in the inclusion shape and some influence of a nonperfect adhesion between the inclusion and the matrix.

Sometimes during the preparation of epoxy resins, air bubbles (or cavities) are formed accidentally. The

TABLE IV
Comparison of the Maximum Values of Principal Stresses Determined for the PVA Inclusion from the Experiment and with Goodier's Theory

Position	σ_1 (MPa)	σ_2 (MPa)	σ_3 (MPa)
Pole (experiment)	−1.4	0.2	−2.8
Pole (Goodier)	−0.8	2.9	−0.8
Equator (experiment)	1.1	10.8	−0.6
Equator (Goodier)	0.8	6.8	0.1

presence of air bubbles also introduces nonuniform stresses into the epoxy matrix. We analyzed the stress state around a small bubble with a radius of 120 μm. Usually, even under small deformation, the shape of the bubble changes from a sphere to an ellipsoid, so we limited the elongation to 0.3%, corresponding to 4.2 MPa of axial tensile stress. The stress components and their direction, determined by the photoelastic method, are presented in Figure 11. A compression of the matrix near the pole (p = 2.1 MPa) and the triaxial tension (negative pressure) at the equator are visible. Here, these tendencies are more evident than for a

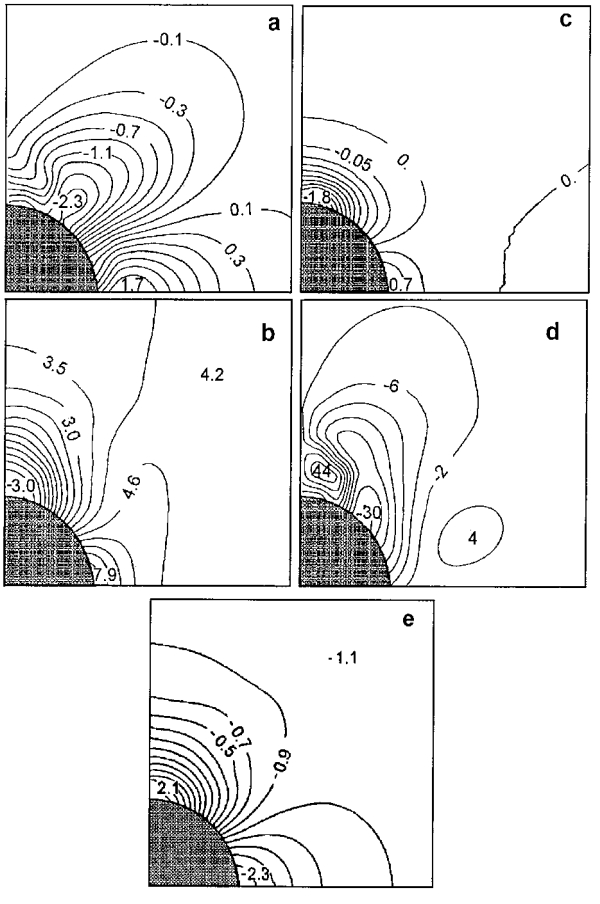

Figure 11 Principal stresses and the direction in an epoxy matrix around an air bubble (the sample was stretched with 4.2 MPa): (a) σ_1, (b) σ_2, (c) σ_3, (d) the angle between the horizontal axis and σ_1 direction, and (e) the pressure.

PVA/epoxy system. They support the explanation based on the relaxation due to the change in the inclusion shape. The pressures at the pole and the equator are comparable, but their signs are opposite, being positive at the pole (compression) and negative at the equator (expansion).

CONCLUSIONS

Microphotoelasticity gives the possibility of determining stresses in systems with small inclusions. The presence of inclusion induces a concentration of stresses in the matrix when an external load is applied. If the adhesion between the matrix and the inclusion is adequate, the range and position of nonuniform stressed zones depend on the relation of the Young's moduli of both components. We studied four types of systems with the same matrix (epoxy resin) and different inclusions that were hard to soft in comparison with the matrix. In the samples with hard inclusions, the tensile stresses concentrated at the pole. For a soft bead, that is, PVA or an air bubble (an air bubble is an example of a bead with infinite compliance), the tensile stresses concentrated at the equator and were partially relaxed at the pole. The soft inclusion promoted stress relaxation by the change in its shape. In the matrix with inclusions such as steel or glass beads, we observed debonding near the pole under relatively low total deformation (2–3%). This fast process significantly changed the stress distribution. Stresses concentrated near the debonding tips at the interface inclusion matrix. For hard inclusions, the pressure at all points of the interface was negative, and the maximum was found at the pole near the inclusion surface from -6 to -10 MPa. This region was sensitive to the initiation of destruction processes such as cavitation and debonding. The pressure near the debonding tip at the interface inclusion matrix was negative at the quite high level of -12.5 MPa, which promoted further debonding at the tip. For soft inclusions, the pressures at the pole and the equator were comparable, but the signs were opposite, being positive at the pole (compression) and negative at the equator (expansion).

References

1. Goodier, J. Trans Am Soc Mech Eng 1933, 55, 39.
2. Edwards, R. H. J Appl Mech Trans Am Soc Mech Eng 1951, 73, 19.
3. Hashin, Z. J Appl Mech 1991, 58, 444.
4. Guild, F. J.; Young, R. J. J Mater Sci 1989, 24, 298.
5. Guild, F. J.; Young, R. J. J Mater Sci 1989, 24, 2454.
6. van Hartingsveldt, E. A.; van Aartsen, J. J. Polymer 1991, 32, 1482.
7. Vollenberg, P. H. T.; Heikens, D. Polymer 1989, 30, 1656.
8. Vollenberg, P. H. T.; Heikens, D. Polymer 1989, 30, 1663.
9. Boven, G.; Folkersma, R.; Challa, G.; Schouten, A.J.; Bosma, M. Polymer 1992, 33, 83.
10. Zhang, H.; Berglund, L. A. Polym Eng Sci 1993, 33, 100.
11. Abate, G. F.; Heikens, D. Polym Commun 1983, 24, 342.
12. Dally, J. W.; Riley, W. F. Experimental Stress Analysis; McGraw-Hill: New York, 1991.
13. Pawlak, A.; Galeski, A. Polym Eng Sci 1996, 36, 2736.
14. Theocaris, P. S.; Gdoutos, E. E. Matrix Theory of Photoelasticity; Springer-Verlag: Berlin, 1979.
15. Aben, H. Integrated Photoelasticity; McGraw-Hill: New York, 1979.
16. Pawlak, A.; Galeski, A. Polym Eng Sci 1996, 36, 2727.
17. Pawlak, A.; Galeski, A. Opt Eng 1995, 34, 3398.